

Mathematical Modeling of Free-Radical Ethylene Copolymerization in High-Pressure Tubular Reactors

Costas Kiparissides,^{*,†,‡} Apostolos Baltsas,[‡] and Stratos Papadopoulos[‡]

Department of Chemical Engineering, Aristotle University of Thessaloniki,
and Chemical Process Engineering Research Institute, P.O. Box 472, 541 24 Thessaloniki, Greece

John P. Congalidis and John R. Richards

E. I. du Pont de Nemours and Company, P.O. Box 80304, Wilmington, Delaware 19880-0304

Mark B. Kelly and Yi Ye

E. I. du Pont de Nemours and Company, P.O. Box 1089, Orange, Texas 77631

A comprehensive mathematical model is developed for the free-radical copolymerization of ethylene with various comonomers (e.g., vinyl acetate, methyl or ethyl acrylate, and acrylic or methacrylic acid) in high-pressure tubular reactors. Polar copolymers usually exhibit lower crystallinity and yield strength than low-density polyethylene grades and are used for applications requiring flexibility, toughness, stress-cracking resistance, and adhesion to coatings. In the present study, a detailed kinetic mechanism is proposed to describe the molecular and compositional developments in the free-radical copolymerization of ethylene with a comonomer. On the basis of the postulated kinetic mechanism, a system of differential mass balance equations are derived for the various molecular species, total mass, energy, and momentum in the polymerization system. The model equations are coupled with a set of algebraic equations for estimating the thermodynamic and transport properties of the reaction mixture. The number and weight molecular weight and copolymer composition averages, short- and long-chain branching frequencies, etc., are calculated in terms of the leading moments of the bivariate number chain-length distributions of “live” and “dead” copolymer chains. The predictive capabilities of the mathematical model are demonstrated by a direct comparison of the model predictions with industrial experimental data on the reactor temperature profile and pressure, the overall monomer conversion, and the final molecular and compositional properties of copolymers. Simulation and experimental results are presented for different copolymer grades including ethylene–ethyl acrylate, ethylene–methyl acrylate, and ethylene–vinyl acetate copolymers.

Introduction

The large number of applications (e.g., packaging, adhesives, coatings, films, etc.)¹ of low-density polyethylene (LDPE) and its copolymers is the result of the wide range of molecular and structural properties of the various homopolymer and copolymer grades. LDPE and its copolymers have been commercially produced in high-pressure reactors for more than 4 decades. The unique properties of LDPE and its copolymers suggest that the demand for these specialty grades will remain strong in the near future.

Two reactor technologies (i.e., tubular and autoclaves) are employed in the high-pressure (co)polymerization of ethylene. The copolymerization of ethylene with a comonomer is typically carried out at very high temperatures (140–300 °C) and pressures (1500–3000 atm). Thus, in the presence of a mixture of initiators (e.g., peroxides and azo compounds), ethylene and a comonomer (e.g., vinyl acetate, acrylic or methacrylic acid, and methyl or ethyl acrylate) can be copolymerized via a free-radical mechanism.

A high-pressure LDPE tubular reactor typically consists of a spiral-wrapped metallic pipe, with a large length-to-diameter ratio. The total length of the tube ranges from 500 to 1500 m, while its internal diameter does not exceed 70–80 mm. With respect to the process heat requirements, the tubular reactor is divided into a number of zones (i.e., preheating, reaction, and coolant zones). In the preheating zones, the ethylene–comonomer feed stream is heated (by steam or water) up to a temperature at which the polymerization is initiated via the thermal decomposition of initiators. The tubular reactor also includes a number of reaction and cooling zones, arranged in a certain sequence, in accordance with the reactor design and product specifications. A commercial tubular reactor usually consists of 2–6 reactor zones and 6–12 coolant zones. Ethylene polymerization is a highly exothermic reaction. The heat of reaction is partially removed through the reactor wall by the heat-transfer fluid (usually water). Approximately half of the reaction heat is removed by the coolant streams flowing in the reactor jacket co- or countercurrently to the reaction fluid. This results in a nonisothermal reactor operation. The temperatures and flow rates of the coolant streams are used to control the heat removal rate and, thus, the temperature profile along the tube.

A schematic representation of a multizone high-pressure tubular reactor is depicted in Figure 1. The

* To whom correspondence should be addressed. Tel.: +30 2310996211. Fax: +30 2310996198. E-mail: cypress@cperi.certh.gr.

[†] Department of Chemical Engineering, Aristotle University of Thessaloniki.

[‡] Chemical Process Engineering Research Institute.

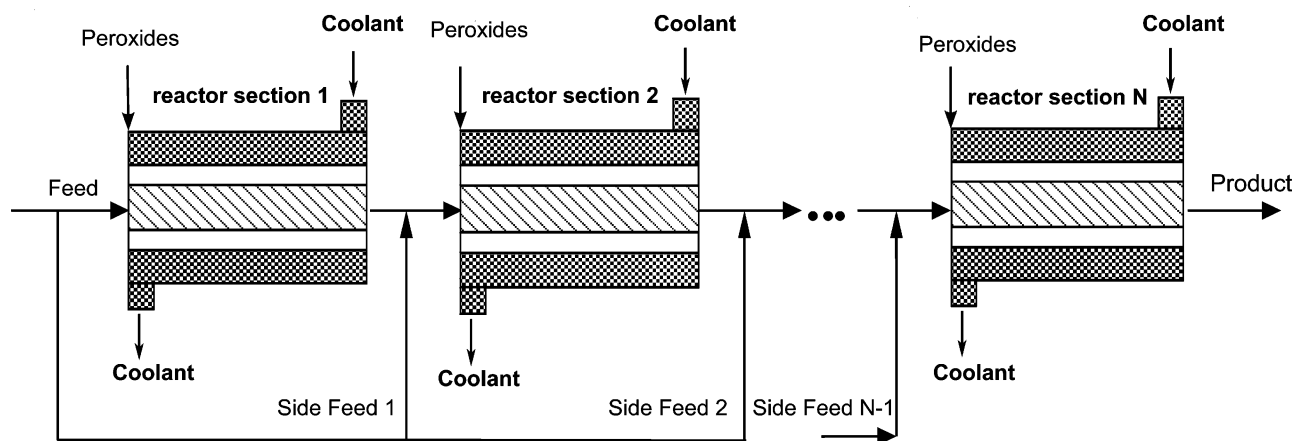


Figure 1. Schematic representation of a multizone high-pressure tubular reactor.

tubular reactor usually includes a number of monomer, initiator, and chain-transfer-agent (CTA) side injection points to control the process conditions, reactor productivity, and final polymer quality. The various initiator feed streams usually consist of mixtures of two to four initiators, having different decomposition temperatures. The selection of an initiator mixture (i.e., initiator half-life times and respective concentrations) depends on the desired conversion range. CTAs are commonly employed to control the molecular weight of the polymer and, therefore, its end-use properties. In conclusion, operating conditions are varied to obtain polymers with a wide range of molecular and compositional properties. In general, a multitude of polyethylene (PE) grades can be produced from a single reactor line. Typical monomer conversions vary in the range of 20–35%. The polymer density ranges from 0.915 to 0.935 g/cm³.

The industrial importance of high-pressure tubular reactor technology has led to extensive studies on reactor modeling over the past 30 years. Thus, a large number of mathematical models^{2–12} on high-pressure polymerization of ethylene in tubular reactors have been published. However, there are only a limited number of papers on modeling and experimental validation of ethylene copolymerization in high-pressure tubular reactors. Zabinsky et al.¹³ studied the ethylene–vinyl acetate copolymerization in high-pressure tubular reactors using the pseudokinetic rate constants method. Verros et al.¹⁴ presented a mathematical model for the copolymerization of ethylene–vinyl acetate in a tubular reactor and studied the effects of operating conditions on the reactor performance and product quality. In the review article of Kiparissides et al.,¹⁵ the modeling of high-pressure ethylene (co)polymerization in high-pressure tubular and autoclave reactors is discussed in detail.

Becker and Busch¹⁶ studied the copolymerization of ethylene with acrylate monomers in an ideally mixed vessel. They developed a penultimate kinetic model to describe the copolymerization of ethylene with methyl acrylate or butyl acrylate. They used sets of independently determined rate coefficients to calculate the total monomer(s) conversion and the copolymer composition. Their model predictions were in good agreement with available experimental measurements. Van Boxtel and Busch¹⁷ investigated the copolymerization of ethylene with methyl acrylate and described an experimental strategy to calculate the values of the kinetic rate parameters. It was found that the postulated kinetic

model was capable of describing the experimental molecular weight distributions and long- (LCB) and short-chain branching (SCB) frequencies of copolymers. In a recent paper by Busch,¹⁸ the latest advances in kinetic modeling and prediction of molecular and structural properties in high-pressure ethylene copolymerization reactors are discussed.

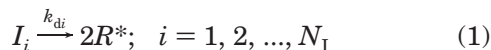
The paper is organized as follows: In the second section, the kinetic mechanism of copolymerization of ethylene with a comonomer is reviewed and the net production/consumption rate functions of all of the molecular species present in the polymerization system are derived. The number and weight molecular weight and copolymer composition averages, SCB and LCB frequencies, etc., are calculated in terms of the leading moments of the bivariate number chain-length distributions of “live” and “dead” copolymer chains. In the third section, a comprehensive reactor model is derived to calculate the temperature and pressure profiles in the tube, the monomer conversions, and the molecular and structural properties of the copolymer chains. Issues related with the estimation of the various kinetic rate constants are also discussed. Finally, in the fourth section, the online tuning of the model to real-time plant data is examined. The predictive capabilities of the mathematical model are demonstrated by a direct comparison of the model predictions with industrial experimental data on the reactor temperature profile, the overall monomer conversion, and the final molecular and compositional properties of the copolymer. Simulation and experimental results are presented for different copolymer grades including ethylene–ethyl acrylate, ethylene–methyl acrylate, and ethylene–vinyl acetate copolymers.

Kinetic Mechanism and Copolymerization Rate Functions

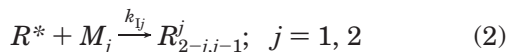
Copolymers made by free-radical copolymerization are typically mixtures of macromolecules with different molecular structural characteristics (e.g., copolymer composition, chain length, and SCB and LCB frequencies). Because the molecular features of the produced polymers are directly related to their end-use properties, control of the copolymer chain microstructure during polymerization is of profound importance. This presupposes a thorough understanding of the polymerization kinetics. In the present study, a comprehensive kinetic mechanism is postulated to describe the free-radical

copolymerization of ethylene with a comonomer (e.g., vinyl acetate, methyl or ethyl acrylate, and acrylic or methacrylic acid). The following elementary reactions are considered:

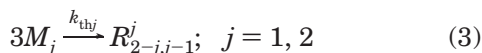
Initiator(s) decomposition



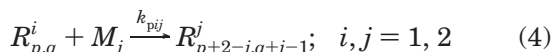
Chain initiation reactions



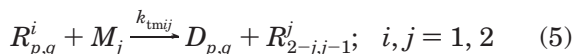
Thermal initiation reactions



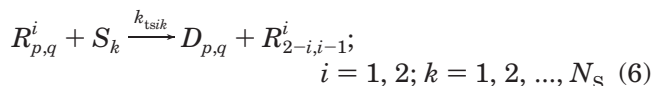
Chain propagation reactions



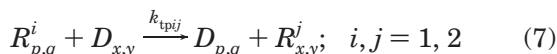
Transfer to monomer



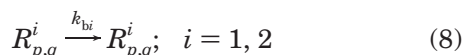
Transfer to CTAs



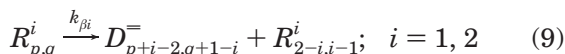
Transfer to polymer (LCB)



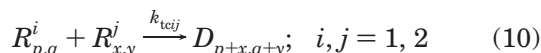
Intramolecular chain transfer (SCB)



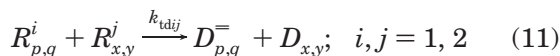
β scission of secondary and tertiary radicals



Termination by combination



Termination by disproportionation



The above kinetic mechanism includes the initiator decomposition and chain initiation reactions, thermal initiation, chain propagation and termination, transfer reactions to monomer and to CTAs, LCB formation by transfer to polymer, SCB formation via intramolecular transfer (backbiting), and β scission of secondary and tertiary radicals. It should be mentioned that ethylene and comonomer decomposition reactions have been included in the kinetic model to take into account reactor runaway phenomena. The symbols I , R^* , M_j ($j = 1, 2$), and S_k ($k = 1, 2, \dots, N_S$) denote the initiator, primary radicals, monomer, and CTA molecules, respectively. The symbols $R_{p,q}^i$ and $D_{p,q}$ identify the “live” and “dead” copolymer chains, respectively. The subscripts p and q denote the corresponding degrees of polymerization for monomers M_1 and M_2 . Finally, the superscript i refers to the ultimate monomer unit in the “live” polymer chains, which can be either of type M_1 or M_2 .

Intramolecular chain-transfer reactions can lead to the formation of short-chain branches. According to Roedel's backbiting mechanism, a growing polymer chain can curl back on its own chain, occasionally transferring the radical activity to the third or fifth carbon atom from its growing end. The principal types of short-chain branches in LDPE are n -butyl and ethyl, with possible formation of n -amyl and n -hexyl branches in smaller amounts. SCB affects the morphology and solid-state properties (e.g., density and crystalline melting point) of PE. LDPE usually contains 10–40 short-chain branches per 1000 carbon atoms. Because the available information on the exact scission mechanism of highly branched copolymer chains is limited, it was assumed for modeling simplification that chain scission occurred at the growing end of “live” copolymer chains.

Long-chain branches are primarily formed by intermolecular chain-transfer reactions. LCB can arise from the abstraction by a “live” polymer chain of a hydrogen atom from the backbone of a “dead” polymer chain, followed by monomer addition to the new radical site. LCB is mainly responsible for the broad molecular weight distribution of LDPE and its rheological behavior. Pladis and Kiparissides¹⁹ reported that the formation of LCB in LDPE via terminal double-bond polymerization was limited to 5–10% of the total LCB content. Thus, in the present study, terminal double-bond polymerization was not included in the kinetic model.

The rate of formation of vinyl groups ($-\text{CH}=\text{CH}_2$) by β scission of the secondary radicals will be higher than the respective rates of formation by termination by disproportionation and chain transfer to monomer reactions. Similarly, the formation of vinylidene groups ($>\text{C}=\text{CH}_2$) can be explained by the scission reaction of the tertiary radicals. The formation of *trans*-vinylene groups ($-\text{CH}=\text{CH}-$) has also been reported, but their concentration is lower than that of the other two unsaturated groups.¹⁵

Copolymerization Rate Functions. The respective net production rates for “live” and “dead” copolymer chains can be obtained by combining the reaction rates of all of the relevant elementary reactions, describing the generation and/or consumption of “live” and “dead” polymer chains. On the basis of the postulated kinetic mechanism, the following general rate functions for “live” and “dead” copolymer chains can be derived:^{14,15}

Net production rate of “live” copolymer chains ending in monomer 1

$$\begin{aligned} r_{R_{p,q}^1} = & \delta(p-1,q) [k_{I1}R^*M_1 + k_{th1}M_1^3 + (k_{tm11}R^1 + \\ & k_{tm21}R^2)M_1 + \sum_{i=1}^{N_S} k_{ts1i}R^1S_i + (k_{\beta 1} + k'_{\beta 1})R^1] + \\ & k_{p11}M_1(R_{p-1,q}^1 - R_{p,q}^1) - k_{p12}M_2R_{p,q}^1 + k_{p21}M_1R_{p-1,q}^2 - \\ & (k_{tm11}M_1 + k_{tm12}M_2)R_{p,q}^1 - \sum_{i=1}^{N_S} (k_{ts1i}S_iR_{p,q}^1) - \\ & k_{tp11}R_{p,q}^1 \sum_{x=1}^{\infty} \sum_{y=1}^{\infty} xD_{x,y} - k_{tp12}R_{p,q}^1 \sum_{x=1}^{\infty} \sum_{y=1}^{\infty} yD_{x,y} + \\ & k_{tp11}R^1pD_{p,q} + k_{tp21}R^2pD_{p,q} - (k_{\beta 1} + k'_{\beta 1})R_{p,q}^1 - \\ & (k_{tc11} + k_{td11})R_{p,q}^1R_{p,q}^1 - (k_{tc12} + k_{td12})R_{p,q}^1R_{p,q}^1 \quad (12) \end{aligned}$$

Net production rate of "live" copolymer chains ending in monomer 2

$$\begin{aligned}
 r_{R_{p,q}^2} = & \delta(p,q-1) [k_{12}R^*M_2 + k_{th2}M_2^3 + (k_{tm12}R^1 + \\
 & k_{tm22}R^2)M_2 + \sum_{i=1}^{N_S} k_{ts2i}R^2S_i + (k_{\beta2} + k'_{\beta2})R^2] + \\
 & k_{p12}M_2R_{p,q-1}^1 - k_{p21}M_1R_{p,q}^2 + k_{p22}M_2(R_{p,q-i}^2 - R_{p,q}^2) - \\
 & (k_{tm21}M_1 + k_{tm22}M_2)R_{p,q}^2 - \sum_{i=1}^{N_S} (k_{ts2i}S_iR_{p,q}^2) - \\
 & k_{tp21}R_{p,q}^2 \sum_{x=1}^{\infty} \sum_{y=1}^{\infty} xD_{x,y} - k_{tp22}R_{p,q}^2 \sum_{x=1}^{\infty} \sum_{y=1}^{\infty} yD_{x,y} + \\
 & k_{tp12}R^1qD_{p,q} + k_{tp22}R^2qD_{p,q} - (k_{\beta2} + k'_{\beta2})R_{p,q}^2 - \\
 & (k_{tc12} + k_{td12})R^1R_{p,q}^2 - (k_{tc22} + k_{td22})R^2R_{p,q}^2 \quad (13)
 \end{aligned}$$

Net production rate of "dead" copolymer chains

$$\begin{aligned}
 r_{D_{p,q}} = & (k_{tm11}M_1 + k_{tm12}M_2)R_{p,q}^1 + (k_{tm21}M_1 + \\
 & k_{tm22}M_2)R_{p,q}^2 + \sum_{i=1}^{N_S} (k_{ts1i}R_{p,q}^1 + k_{ts2i}R_{p,q}^2)S_i + \\
 & (k_{tp11} \sum_{x=1}^{\infty} \sum_{y=1}^{\infty} xD_{x,y} + k_{tp12} \sum_{x=1}^{\infty} \sum_{y=1}^{\infty} yD_{x,y})R_{p,q}^1 + \\
 & (k_{tp21} \sum_{x=1}^{\infty} \sum_{y=1}^{\infty} xD_{x,y} + k_{tp22} \sum_{x=1}^{\infty} \sum_{y=1}^{\infty} yD_{x,y})R_{p,q}^2 - \\
 & (k_{tp11}pD_{p,q} + k_{tp12}qD_{p,q})R^1 - (k_{tp21}pD_{p,q} + \\
 & k_{tp22}qD_{p,q})R^2 + (k_{\beta1} + k'_{\beta1})R_{p+1,q}^1 + (k_{\beta2} + \\
 & k'_{\beta2})R_{p,q+1}^2 + k_{td11}R^1R_{p,q}^1 + k_{td12}(R^1R_{p,q}^2 + R^2R_{p,q}^1) + \\
 & k_{td22}R^2R_{p,q}^2 + \frac{1}{2}k_{tc11} \sum_{x=1}^{p-1} \sum_{y=1}^{q-1} R_{x,y}^1 R_{p-x,q-y}^1 + \\
 & k_{tc12} \sum_{x=1}^{p-1} \sum_{y=1}^{q-1} R_{x,y}^1 R_{p-x,q-y}^2 + \frac{1}{2}k_{tc22} \sum_{x=1}^{p-1} \sum_{y=1}^{q-1} R_{x,y}^2 R_{p-x,q-y}^2 \quad (14)
 \end{aligned}$$

where $\delta(p,q)$ is Kronecker's delta function and is given by

$$\delta(p,q) = \delta(p)\delta(q); \quad \delta(i) = \begin{cases} 1 & \text{for } i = 0 \\ 0 & \text{for } i \neq 0 \end{cases} \quad (15)$$

and R^i denotes the total concentration of "live" polymer chains of type i :

$$R^i = \sum_{p=1}^{\infty} \sum_{q=1}^{\infty} R_{p,q}^i; \quad i = 1, 2 \quad (16)$$

Moment Rate Functions. On the basis of the above definitions for the rate functions of all of the molecular species $R_{p,q}^i$ and $D_{p,q}$ present in the system, an extremely large number of molecular species balances (e.g., assuming p and q can take values up to 20 000) need to be derived to describe the molecular weight and

compositional developments in the copolymerization reactor. Thus, the method of double moments¹⁵ was utilized to reduce the infinite system of molar balance equations into a low-order system of differential moment equations that can easily be solved. The method of moments is based on the statistical representation of the average molecular weight and compositional properties of the polymer in terms of the leading moments of the number chain-length distributions of "live" and "dead" copolymer chains. In this study, the bivariate number chain-length distributions for $R_{p,q}^i$ and $D_{p,q}$ associated with the "live" and "dead" copolymer chains were employed. Accordingly, the respective moments for "live" and "dead" copolymer chains are defined:

$$\lambda_{m,n}^i = \sum_{p=0}^{\infty} \sum_{q=0}^{\infty} p^m q^n R_{p,q}^i; \quad m, n = 0, 1, 2; i = 1, 2 \quad (17)$$

$$\mu_{m,n} = \sum_{p=0}^{\infty} \sum_{q=0}^{\infty} p^m q^n D_{p,q}; \quad m, n = 0, 1, 2 \quad (18)$$

where $p + q \geq 1$. The relevant rate functions for the moments $\lambda_{m,n}^i$ and $\mu_{m,n}$ are then obtained from eqs 12–14 by multiplying each term by $p^m q^n$ and summing the resulting expressions over the total variations of p and q . The final equations for the corresponding moment rate functions are as follows:

Moment rates for "live" copolymer chains

$$\begin{aligned}
 r_{\lambda_{m,n}^1} = & \delta(n) [k_{11}R^*M_1 + k_{th1}M_1^3 + (k_{tm11}\lambda_{0,0}^1 + \\
 & k_{tm21}\lambda_{0,0}^2)M_1 + \sum_{i=1}^{N_S} k_{ts1i}\lambda_{0,0}^1S_i + (k_{\beta1} + k'_{\beta1})\lambda_{0,0}^1] + \\
 & k_{p11}M_1 \sum_{i=0}^m \binom{m}{i} \lambda_{m-i,n}^1 - k_{p11}M_1 \lambda_{m,n}^1 - k_{p12}M_2 \lambda_{m,n}^1 + \\
 & k_{p21}M_1 \sum_{i=0}^m \binom{m}{i} \lambda_{m-i,n}^2 - (k_{tm11}M_1 + k_{tm12}M_2) \lambda_{m,n}^1 - \\
 & \sum_{i=1}^{N_S} (k_{ts1i}S_i \lambda_{m,n}^1) - k_{tp11}\mu_{1,0}\lambda_{m,n}^1 - k_{tp12}\mu_{0,1}\lambda_{m,n}^1 + \\
 & k_{tp11}\lambda_{0,0}^1\mu_{m+1,n} + k_{tp21}\lambda_{0,0}^2\mu_{m+1,n} - (k_{\beta1} + k'_{\beta1})\lambda_{m,n}^1 - \\
 & (k_{tc11} + k_{td11})\lambda_{0,0}^1\lambda_{m,n}^1 - (k_{tc12} + k_{td12})\lambda_{0,0}^2\lambda_{m,n}^1 \quad (19)
 \end{aligned}$$

$$\begin{aligned}
 r_{\lambda_{m,n}^2} = & \delta(m) [k_{12}R^*M_2 + k_{th2}M_2^3 + (k_{tm12}\lambda_{0,0}^1 + \\
 & k_{tm22}\lambda_{0,0}^2)M_2 + \sum_{i=1}^{N_S} k_{ts2i}\lambda_{0,0}^2S_i + (k_{\beta2} + k'_{\beta2})\lambda_{0,0}^2] + \\
 & k_{p12}M_2 \sum_{i=0}^n \binom{n}{i} \lambda_{m,n-i}^1 - k_{p21}M_1 \lambda_{m,n}^2 + k_{p22}M_2 \\
 & \sum_{i=0}^n \binom{n}{i} \lambda_{m,n-i}^2 - k_{p22}M_2 \lambda_{m,n}^2 - (k_{tm21}M_1 + k_{tm22}M_2) \lambda_{m,n}^2 - \\
 & \sum_{i=1}^{N_S} (k_{ts2i}S_i \lambda_{m,n}^2) - k_{tp21}\mu_{1,0}\lambda_{m,n}^2 - k_{tp22}\mu_{0,1}\lambda_{m,n}^2 + \\
 & k_{tp12}\lambda_{0,0}^1\mu_{m,n+1} + k_{tp22}\lambda_{0,0}^2\mu_{m,n+1} - (k_{\beta2} + k'_{\beta2})\lambda_{m,n}^2 - \\
 & (k_{tc12} + k_{td12})\lambda_{0,0}^1\lambda_{m,n}^2 - (k_{tc22} + k_{td22})\lambda_{0,0}^2\lambda_{m,n}^2 \quad (20)
 \end{aligned}$$

Moment rates for “dead” copolymer chains

$$\begin{aligned}
r_{\mu_{m,n}} = & (k_{tm11}M_1 + k_{tm12}M_2)\lambda_{m,n}^1 + (k_{tm21}M_1 + \\
& k_{tm22}M_2)\lambda_{m,n}^2 + \sum_{i=1}^{N_S} (k_{ts1i}\lambda_{m,n}^1 + k_{ts2i}\lambda_{m,n}^2)S_i + \\
& k_{tp11}\mu_{1,0}\lambda_{m,n}^1 + k_{tp12}\mu_{0,1}\lambda_{m,n}^1 + k_{tp21}\mu_{1,0}\lambda_{m,n}^2 + \\
& k_{tp22}\mu_{0,1}\lambda_{m,n}^2 - k_{tp11}\lambda_{0,0}^1\mu_{m+1,n} - k_{tp12}\lambda_{0,0}^1\mu_{m,n+1} - \\
& k_{tp21}\lambda_{0,0}^2\mu_{m+1,n} - k_{tp22}\lambda_{0,0}^2\mu_{m,n+1} + (k_{\beta 1} + \\
& k'_{\beta 1})\sum_{i=0}^m \binom{m}{i}(-1)^i\lambda_{m-i,n}^1 + (k_{\beta 2} + k'_{\beta 2})\sum_{i=0}^n \binom{n}{i}(-1)^i\lambda_{m,n-i}^2 + \\
& k_{td11}\lambda_{0,0}^1\lambda_{m,n}^1 + k_{td12}\lambda_{0,0}^1\lambda_{m,n}^2 + k_{td12}\lambda_{0,0}^2\lambda_{m,n}^1 + \\
& k_{td22}\lambda_{0,0}^2\lambda_{m,n}^2 + 1/2k_{tc11}\sum_{i=0}^m\sum_{j=0}^n \binom{m}{i}\binom{n}{j}\lambda_{i,j}^1\lambda_{m-i,n-j}^1 + \\
& k_{tc12}\sum_{i=0}^m\sum_{j=0}^n \binom{m}{i}\binom{n}{j}\lambda_{i,j}^1\lambda_{m-i,n-j}^2 + \\
& 1/2k_{tc22}\sum_{i=0}^m\sum_{j=0}^n \binom{m}{i}\binom{n}{j}\lambda_{i,j}^2\lambda_{m-i,n-j}^2 \quad (21)
\end{aligned}$$

It should be pointed out that when transfer to polymer reactions is included in the kinetic mechanism, the $\mu_{m,n}$ -order moment equations for “dead” copolymer chains will depend on higher-order moments. To eliminate this dependence, several closure methods have been proposed in the literature.¹³ In the present study, the bulk²⁰ moment rate equations, defined in terms of the moments of “live” and “dead” copolymer chains ($\mu'_{m,n} = \mu_{m,n} + \lambda_{m,n}^1 + \lambda_{m,n}^2$), were employed. Thus, by addition of eqs 19 and 20 to eq 21, the following equation for $r_{\mu'_{m,n}}$ is obtained.

$$\begin{aligned}
r_{\mu'_{m,n}} = & \delta(n)(k_{I1}M_1R^* + k_{th1}M_1^3 + (k_{tm11}\lambda_{0,0}^1 + \\
& k_{tm21}\lambda_{0,0}^2)M_1 + (k_{\beta 1} + k'_{\beta 1})\lambda_{0,0}^1 + \sum_{i=1}^{N_S} k_{ts1i}\lambda_{0,0}^1S_i) + \\
& \delta(m)(k_{I2}M_2R^* + k_{th2}M_2^3 + (k_{tm12}\lambda_{0,0}^1 + k_{tm22}\lambda_{0,0}^2)M_2 + \\
& (k_{\beta 2} + k'_{\beta 2})\lambda_{0,0}^2 + \sum_{i=1}^{N_S} k_{ts2i}\lambda_{0,0}^2S_i) + k_{p11}M_1(\sum_{i=0}^m \binom{m}{i}\lambda_{m-i,n}^1 - \\
& \lambda_{m,n}^1) + k_{p12}M_2(\sum_{i=0}^n \binom{n}{i}\lambda_{m,n-i}^1 - \lambda_{m,n}^1) + \\
& k_{p21}M_1(\sum_{i=0}^m \binom{m}{i}\lambda_{m-i,n}^2 - \lambda_{m,n}^2) + k_{p22}M_2(\sum_{i=0}^n \binom{n}{i}\lambda_{m,n-i}^2 - \\
& \lambda_{m,n}^2) + (k_{\beta 1} + k'_{\beta 1})(\sum_{i=0}^m \binom{m}{i}(-1)^i\lambda_{m-i,n}^1 - \lambda_{m,n}^1) + (k_{\beta 2} + \\
& k'_{\beta 2})(\sum_{i=0}^n \binom{n}{i}(-1)^i\lambda_{m,n-i}^2 - \lambda_{m,n}^2) + \\
& 1/2k_{tc11}(\sum_{i=0}^m\sum_{j=0}^n \binom{m}{i}\binom{n}{j}\lambda_{i,j}^1\lambda_{m-i,n-j}^1 - 2\lambda_{0,0}^1\lambda_{m,n}^1) + \\
& 1/2k_{tc22}(\sum_{i=0}^m\sum_{j=0}^n \binom{m}{i}\binom{n}{j}\lambda_{i,j}^2\lambda_{m-i,n-j}^2 - 2\lambda_{0,0}^2\lambda_{m,n}^2) + \\
& k_{tc12}(\sum_{i=0}^m\sum_{j=0}^n \binom{m}{i}\binom{n}{j}\lambda_{i,j}^1\lambda_{m-i,n-j}^2 - \lambda_{0,0}^1\lambda_{m,n}^1 - \lambda_{0,0}^2\lambda_{m,n}^2) \quad (22)
\end{aligned}$$

Molecular Species Rate Functions. Similarly, on the basis of the above kinetic mechanism, the following molecular species rate functions for initiator(s), monomer(s), etc., can be derived:

Initiator(s) consumption rate(s)

$$r_{di} = k_{di}I_i; \quad i = 1, \dots, N_I \quad (23)$$

Primary radicals formation rate

$$r_R = \sum_{i=1}^{N_i} 2f_i k_{di}I_i - (\sum_{i=1}^2 k_{ti}M_i)R^* \quad (24)$$

Monomer consumption rates

$$\begin{aligned}
r_{M_i} = & k_{ti}M_iR^* + k_{thi}M_i^3 + [(k_{pi} + k_{tmi})\lambda_{0,0}^1 + \\
& (k_{pi} + k_{tmi})\lambda_{0,0}^2]M_i; \quad i = 1, 2 \quad (25)
\end{aligned}$$

CTA consumption rate(s)

$$r_{Si} = (k_{ts1i}\lambda_{0,0}^1 + k_{ts2i}\lambda_{0,0}^2)S_i; \quad i = 1, \dots, N_S \quad (26)$$

Reactor Design Equations

To derive the relevant design equations, describing the copolymerization of ethylene with a comonomer in a multizone, multifeed high-pressure tubular reactor, the following simplifying assumptions were made: (i) the reaction mixture is treated as one phase system; (ii) plug-flow conditions and the absence of axial mixing (this assumption is well justified for tubular reactors operating at high Reynolds numbers) are assumed; (iii) accumulation terms are negligible; (iv) heat effects due to chain initiation, termination, and transfer reactions are negligible (i.e., the polymerization heat is only assigned to propagation reactions); (v) the terminal kinetic model of copolymerization is employed (i.e., penultimate monomer effects are negligible). A justification of these assumptions is given by Kiparissides et al.¹⁵

A comprehensive mathematical model for a high-pressure ethylene copolymerization tubular reactor includes a number of differential molecular species, energy and momentum balances, and a system of algebraic equations for the estimation of physical, thermodynamic, and transport properties of the reaction mixture. In the present study, a set of steady-state differential equations for the molar rates of the various species in the reactor were derived. The molar flow rate of species j was expressed in terms of the fluid velocity, u , and the corresponding molar concentration of species j :

$$F_j = AuC_j = (\pi d_i^2/4)uC_j \quad (27)$$

where A is the cross-sectional area of the tube. Accordingly, the following design equations were derived for each reactor zone of the multizone tubular reactor.

Initiator balance(s)

$$dF_{I_i}/dV = -r_{I_i}; \quad i = 1, 2, \dots, N_I \quad (28)$$

Primary radicals balance

$$dF_{R^*}/dV = r_{R^*} \quad (29)$$

Monomer balances

$$dF_{M_i}/dV = -r_{M_i}; \quad i = 1, 2 \quad (30)$$

CTA balance(s)

$$dF_{S_i}/dV = -r_{S_i}; \quad i = 1, 2, \dots, N_S \quad (31)$$

"Live" copolymer moment balances

$$dF_{\lambda_{m,n}^i}/dV = r_{\lambda_{m,n}^i}; \quad i = 1, 2 \quad (32)$$

"Bulk" copolymer moment balances

$$dF_{\mu'_{m,n}}/dV = r_{\mu'_{m,n}} \quad (33)$$

SCB balance

$$dF_{SCB}/dV = k_{b1}\lambda_{0,0}^1 + k_{b2}\lambda_{0,0}^2 \quad (34)$$

LCB balance

$$dF_{LCB}/dV = k_{tp11}\lambda_{0,0}^1\mu_{1,0} + k_{tp12}\lambda_{0,0}^1\mu_{0,1} + k_{tp21}\lambda_{0,0}^2\mu_{1,0} + k_{tp22}\lambda_{0,0}^2\mu_{0,1} \quad (35)$$

Vinyl groups balance

$$dF_{VNL}/dV = k_{\beta 1}\lambda_{0,0}^1 + k_{\beta 2}\lambda_{0,0}^2 + \sum_{i=1}^{N_S} (k_{ts1i}\lambda_{0,0}^1 + k_{ts2i}\lambda_{0,0}^2)S_i + (k_{tm11}\lambda_{0,0}^1 + k_{tm21}\lambda_{0,0}^2)M_1 + (k_{tm12}\lambda_{0,0}^1 + k_{tm22}\lambda_{0,0}^2)M_2 + (k_{td11}\lambda_{0,0}^1 + k_{td21}\lambda_{0,0}^2)\lambda_{0,0}^1 + (k_{td12}\lambda_{0,0}^1 + k_{td22}\lambda_{0,0}^2)\lambda_{0,0}^2 \quad (36)$$

Vinylidene groups balance

$$dF_{VND}/dV = k'_{\beta 1}\lambda_{0,0}^1 + k'_{\beta 2}\lambda_{0,0}^2 \quad (37)$$

Momentum balance

$$dP/dV = -(8/\pi d_i^3) f_r \rho_m u^2 \quad (38)$$

Energy balance for the reaction mixture

$$dT/dV = (1/\rho_m u C_p A) \left[\sum_{i=1}^2 (-\Delta H_{ri}) (k_{p1i}\lambda_{0,0}^1 + k_{p2i}\lambda_{0,0}^2) M_i \right] - (4U_i/d_i \rho_m u C_p A) (T - T_c) \quad (39)$$

Energy balance for the coolant in the jacket

$$dT_c/dV = (\pi d_i U_i / \dot{m}_c C_{pc} A') (T - T_c) \quad (40)$$

where A' is the cross section of the reactor-jacket annulus.

Molecular Properties. The various molecular weight averages, the LCB and SCB per 1000 carbon atoms, and the numbers of vinyl and vinylidene double bonds were expressed in terms of the leading moments of the bivariate chain-length distribution:

Number-average molecular weight (M_n)

$$M_n = (MW_1 F_{\mu'_{1,0}} + MW_2 F_{\mu'_{0,1}}) / F_{\mu'_{0,0}} \quad (41)$$

Weight-average molecular weight (M_w)

$$M_w = (MW_1^2 F_{\mu'_{2,0}} + 2MW_1 MW_2 F_{\mu'_{1,1}} + MW_2^2 F_{\mu'_{0,2}}) / (F_{\mu'_{1,0}} MW_1 + F_{\mu'_{0,1}} MW_2) \quad (42)$$

z-average molecular weight (M_z)

$$M_z = \frac{F_{\mu'_{3,0}} MW_1^3 + 3MW_1^2 MW_2 F_{\mu'_{2,1}} + 3MW_1 MW_2^2 F_{\mu'_{1,2}} + MW_2^3 F_{\mu'_{0,3}}}{MW_1^2 F_{\mu'_{2,0}} + 2MW_1 MW_2 F_{\mu'_{1,1}} + MW_2^2 F_{\mu'_{0,2}}} \quad (43)$$

where MW_i is the molecular weight of monomer M_i .

Number of long-chain branches per

10³ carbon atoms

$$LCB/1000C = 500F_{LCB} / (F_{\mu'_{1,0}} + F_{\mu'_{0,1}}) \quad (44)$$

Number of short-chain branches

per 10³ carbon atoms

$$SCB/1000C = 500F_{SCB} / (F_{\mu'_{1,0}} + F_{\mu'_{0,1}}) \quad (45)$$

Number of vinyl double bonds per 10³ carbon atoms

$$VNL/1000C = 500F_{VNL} / (F_{\mu'_{1,0}} + F_{\mu'_{0,1}}) \quad (46)$$

Number of vinylidene double bonds

per 10³ carbon atoms

$$VND/1000C = 500F_{VND} / (F_{\mu'_{1,0}} + F_{\mu'_{0,1}}) \quad (47)$$

Similarly, the cumulative number and weight copolymer composition averages were calculated by the following equations:

Number-average copolymer composition (F_{n1})

$$F_{n1} = F_{\mu'_{1,0}} / (F_{\mu'_{1,0}} + F_{\mu'_{0,1}}) \quad (48)$$

Weight-average copolymer composition (F_{w1})

$$F_{w1} = (MW_1 F_{\mu'_{2,0}} + MW_2 F_{\mu'_{1,1}}) / [MW_1 F_{\mu'_{2,0}} + (MW_1 + MW_2) F_{\mu'_{1,1}} + MW_2 F_{\mu'_{0,2}}] \quad (49)$$

Mass fraction of monomer M_1 in copolymer (CC)

$$CC = MW_1 F_{\mu'_{1,0}} / (MW_1 F_{\mu'_{1,0}} + MW_2 F_{\mu'_{0,1}}) \quad (50)$$

Finally, the copolymer density and melt index (MI) were calculated in terms of M_w , LCB, polydispersity index, and SCB, using experimentally fitted semiempirical correlations.

Physical, Thermodynamic, and Transport Properties. The accurate estimation of the physical, transport, and thermodynamic properties of the reaction mixture is essential to any simulation study of the process. Physical, transport, and thermodynamic properties strongly depend on reactor operating conditions (e.g., temperature, pressure, and concentrations of the various molecular species). For the prediction of thermodynamic properties (i.e., specific volume, specific enthalpy, and specific heat capacity) of monomers and solvents, a generalized correlation, based on a three-parameter corresponding states model,²¹ was employed.

The thermodynamic properties (i.e., specific heat and specific enthalpy) of the polymer were predicted by employing a correlation proposed by Wunderlich and Baur.²²

The solution viscosity of the reaction medium was calculated using a correlation proposed by Mendelson.^{23,24}

$$\eta_s = \eta_{sp} + \eta_0 \exp[(E_v/R)(T^{-1} - T_0^{-1})] \quad (51)$$

where η_{sp} is the viscosity of the pure phase (i.e., monomers and solvents) and η_0 is a reference viscosity at temperature T_0 .

The viscosity of comonomers and solvents, η_{sp} , was calculated using the Joshi Stiel and Thodos²⁵ correlation. Following the original developments of Mendelson, the reference solution viscosity η_0 was expressed in terms of the polymer mass fraction, X_p , and weight-average molecular weight, M_w :

$$\eta_0 = p_3 X_p^{p_4} M_w^{p_5} \quad (52)$$

On the other hand, the activation energy, E_v , was expressed in terms of the polymer mass fraction in the solution:^{23,24}

$$E_v = p_1 \exp(p_2 X_p) \quad (53)$$

The adjustable parameters p_i appearing in eqs 52 and 53 were estimated using the experimental data of Ehrlich and Woodbrey²⁶ on the solution viscosity of ethylene-PE and experimental temperatures and coolant flow rate measurements obtained from the industrial reactor.

The calculation of the overall heat-transfer coefficient was based on the following equation:

$$\frac{1}{U_i} = \frac{1}{h_i} + \frac{d_i \ln(d_o/d_i)}{2k_w} + \frac{d_i}{d_o h_o} + \frac{1}{h_f} \quad (54)$$

where h_o , h_i , and h_f denote the corresponding outside, inside, and wall fouling heat-transfer coefficients. The film heat-transfer coefficients h_i and h_o were calculated in terms of the Nusselt numbers and respective thermal conductivities of the reaction fluid and coolant. The thermal conductivity of the metal wall, k_w , was set equal to 46 W/m·K²⁷ while the value of the wall fouling heat-transfer coefficient, h_f , was estimated from experimental temperature and flow rate measurements (see the following section on online tuning of the model).

Kinetic Rate Constants. One of the most important issues in simulating the operation of a high-pressure reactor is the selection of the numerical values of the kinetic rate constants. Detailed information on the kinetic rate constants for the high-pressure homopolymerization/copolymerization of ethylene can be found in the papers of Goto et al.,⁵ Brandolin et al.,¹² Kiparisides et al.,^{14,15} Busch et al.,^{16–18} and Buback et al.^{28–33}

Needless to say, the accurate experimental determination of the reactivity ratios is a prerequisite to any realistic simulation analysis on copolymerization of ethylene with a comonomer. Buback and co-workers^{30,31} determined experimentally the reactivity ratios of ethylene-methacrylic acid and ethylene-acrylic acid at 2000 bar and temperatures in the range of 240–280 °C. In another study by Buback et al.,²⁸ the reactivity ratios of ethylene-2-ethylhexyl acrylate were experimentally

Table 1. Reactivity Ratios of Ethylene with Various Comonomers^{14,28–32}

comonomer	r_1	r_2	T (°C)	P (atm)
methyl acrylate	0.045 ± 0.002	5.3 ± 0.2	220	2000
ethyl acrylate	0.050 ± 0.002	3.9 ± 0.9	220	2000
butyl acrylate	0.052 ± 0.005	3.4 ± 1.1	220	2000
acrylic acid	0.049	8 ± 2	240	2000
methacrylic acid	0.054	11 ± 3	240	2000
vinyl acetate	1.07	1.09	90	1010

determined. They reported that the values of the reactivity ratios $r_1 = k_{p11}/k_{p12}$ and $r_2 = k_{p22}/k_{p21}$ were equal to 0.05 and 3.9, respectively. Thus, in the copolymerization of ethylene with 2-ethylhexyl acrylate, the acrylate content in the copolymer chains will be higher than the initial feed monomer composition. In a recent publication by Buback and Droge,²⁹ the reactivity ratios of ethylene-methyl acrylate were experimentally determined at high pressure (2000 bar) and temperature (220–290 °C). In Table 1, the reactivity ratios of ethylene with different polar monomers and vinyl acetate (VA) are reported. It is apparent that, in the copolymerization of ethylene with various acrylates and acrylic and methacrylic acid, “live” polymer chains ending in an ethylene radical will favor cross-propagation rather than homopropagation reactions. In contrast, the reactivity ratios for ethylene-vinyl acetate are almost equal, resulting in a uniform copolymer composition.

In this study, most values of the kinetic parameters were taken from previous publications.^{5,14,15,28–33} A limited number of kinetic rate constants were reestimated from available industrial data on temperature profiles, overall monomer conversion, and molecular and structural properties (e.g., M_n , M_w , LCB, copolymer composition, etc.) of various copolymer grades, using an iterative two-step approach. Initially, the kinetic rate constants (e.g., for initiator decomposition, propagation, and termination reactions) were fitted to industrial data on the overall monomer conversion and temperature profiles so that the overall mass and energy balances on the tubular reactor were satisfied. In the second step, the kinetic parameters responsible for the molecular and structural properties of the copolymers were estimated so that the model predictions were in agreement with experimental measurements on M_n , M_w , LCB, overall copolymer composition, etc. This sequential two-step approach was repeated until a global set of kinetic parameters simulating all experimental results could be found. It is important to point out that the number of estimated parameters for each copolymer grade was kept very low (e.g., four to six rate constants). It should be noted that the exact values of all of the kinetic parameters employed in this study are not reported for confidentiality reasons.

Diffusion-Controlled Reactions. Free-radical polymerization reactions can become diffusion-controlled even at low monomer conversions. Buback³⁴ studied both experimentally and theoretically the dependence of the termination and propagation rate constants on monomer conversion in high-pressure polymerization of ethylene. Buback showed that the termination rate constant initially decreases up to 15% ethylene conversion, remains relatively constant up to 60% ethylene conversion, and then sharply decreases up to high monomer conversions. This means that, in a copolymerization kinetic model, the variation of termination rate constants with respect to the overall monomer conver-

sion should be accounted for. In a recent publication,³⁵ a generalized free-volume model was developed for free-radical diffusion-controlled copolymerization reactions. Termination rate constants were expressed in terms of an intrinsic reaction term and a diffusion-limited one:

$$k_{t_{ii}}^{-1} = k_{t_{ii}}^0{}^{-1} + k_{t_{ii}}^d{}^{-1} \quad (55)$$

where $k_{t_{ii}}^0$ is the termination rate constant at very low conversions (i.e., $\sim 1\%$) and $k_{t_{ii}}^d$ is a diffusion-controlled contribution calculated in terms of the diffusion coefficient of the terminating "live" copolymer chains. In this study, the copolymerization diffusion-controlled model of Keramopoulos and Kiparissides³⁵ was employed for the calculation of the $k_{t_{ii}}^d$ term in eq 55.

Implementation and Presentation of the Results

On the basis of the above reactor design equations, a user-friendly software package was developed to simulate the free-radical copolymerization of ethylene with various comonomers in high-pressure tubular reactors. The simulator can account for multiple reaction and cooling zones, multiple injection points for monomers, initiator mixtures, and solvents along the reactor length, and multiple coolant streams, flowing in the reactor jacket in two different modes (i.e., co- and countercurrently to the reaction medium). The simulator also includes a comprehensive library for the estimation of thermodynamic and transport properties of the reaction mixture as well as a parameter estimator for the online tuning of the model.

Online Parameter Estimation. In general, the operation of high-pressure tubular reactors is subject to significant variability, which is gradually manifested during a single polymer grade production. The major sources of this variability are the fouling of the inner surface of the tube due to polymer deposition and the accumulation of reactive impurities due to monomer and solvent recycling.³⁶ During a single polymer grade production, the reactor does not exhibit a typical steady-state operation, for the inner wall of the tube is quickly fouled because of polymer deposition. The fouling of a reactor zone is partially overcome by a periodic increase of the reactor pressure by means of a control valve located at the reactor exit. The pulse motion of the valve results in an increase of the flow velocity, which tears away the polymeric deposits. However, the actual defouling of a reactor zone is principally effected by increasing the inlet temperature of the coolant in the relevant reactor jackets, which results in the melting of the polymer wall deposits. The time scale of the fouling–defouling cycles of the reactor operation is about 2–10 h.

The reactor wall fouling ($R_f = h_f^{-1}$) was represented as a variable heat-transfer resistance term in the calculation of the overall heat-transfer coefficient (see eq 54). It should be pointed out that, by increasing the reactor fouling, the overall heat-transfer coefficient decreases, resulting in an increase of the reactor temperature profile. Because the polymer properties are to a great extent determined by the operating conditions in the reactor, even small variations in the reactor temperature profile due to fouling can result in significant changes in monomer conversion and molecular properties of the polymer. Furthermore, because of recycling of the unreacted raw materials, impurities are

accumulated in the system. The impurities, depending on their nature, can act as either CTAs (methane), radical generators (oxygen), or inhibitors deactivating the primary radicals produced by the decomposition of the initiators. Also, the actual initiator pump output, and consequently the initiator flow rate into a reaction zone, can be subjected to some variations.

In general, the operation of the tubular reactor will be influenced by the presence of time-varying process disturbances (e.g., fouling and impurities) that are slow and persistent because it takes hours for their gradual buildup. On the other hand, very fast chemical reactions, taking place in the reactor, result in fast reactor dynamics. Therefore, the use of an online parameter estimator that will make the mathematical model adaptive to the process variability and predictive of the reactor performance is needed.

In this work, an adaptive parameter estimator technique was developed, based on the appropriate measurements from the reactor, for the online estimation of certain key model parameters, so that the tuned model can be used for real-time optimization of the reactor performance. The selected adjustable model parameters were as follows: (i) the overall initiator efficiency that affects the concentration of the primary radicals and, thus, the polymerization rate and the heat released in the reaction zones and (ii) the fouling factor of the inner surface of the tube wall that controls the heat-transfer rate in the coolant zones.

Typical measurements in a high-pressure tubular reactor include reaction and coolant temperature profiles, conversion, melt flow index, and polymer density. Regarding the selection of reactor measurements for the online parameter estimator, the temperature profile along the tube length and the coolant temperatures in each zone were chosen for estimating the adjustable model parameters. The parameter estimation was carried out by minimizing the following objective function:

$$J = \sum_{i=1}^N w_i (T_{c,i} - T_{e,i})^2 \quad (56)$$

where w_i is the weight for the i th temperature measurement and $T_{c,i}$ and $T_{e,i}$ are the calculated (by the model) and experimental temperatures, respectively. The parameter estimation problem was solved for each reaction/cooling zone in a sequential way.³⁶

The mathematical model for the high-pressure LDPE copolymerization reactor consists of a system of stiff, nonlinear ordinary differential equations for the leading moments ($\lambda_{m,n}^i$; $\mu_{m,n}^i$; $m, n = 0, 1, 2$; $i = 1, 2$) of the bivariate number chain-length distributions of "live" and "dead" copolymer chains as well as a set of differential equations governing the conservation of all other molecular species. The combined system of differential and algebraic equations for the thermodynamic and physical transport properties of the reaction mixture were numerically solved using the DGEAR routine of the IMSL³⁷ numerical library. For the parameter estimator problem, the IMSL DUVMGs routine was employed.

Model and Experimental Results. The industrial reactor consisted of a number of reactor sections (two or three) depending on the number of initiator injection points. Each reactor section was divided into a number of reaction and cooling zones. The total flow rate of monomers (ethylene and comonomer) and solvents was split into two feed streams, namely, a front feed stream

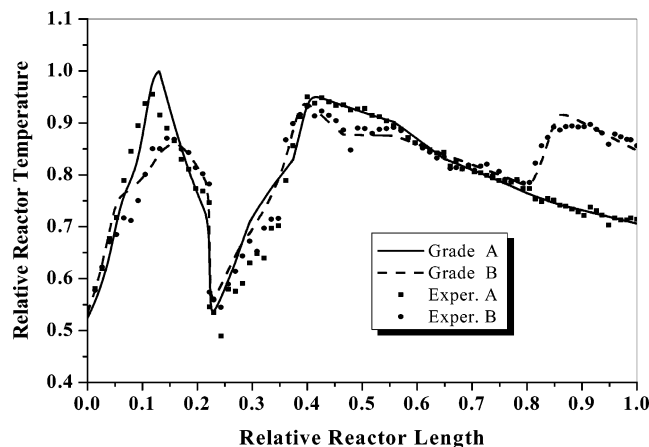


Figure 2. Predicted vs measured temperature profiles for two EEA copolymer grades (A and B).

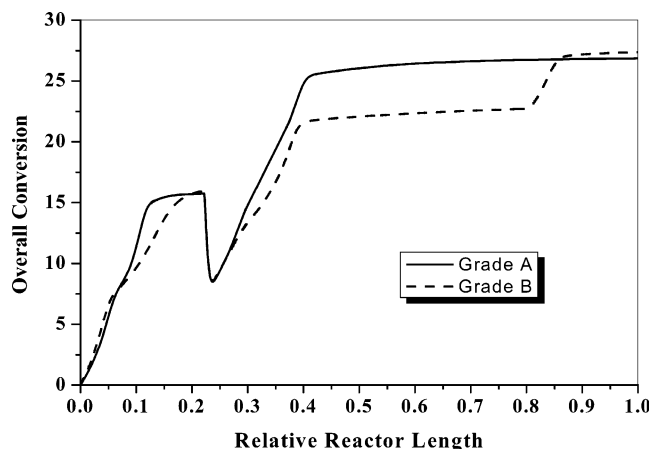


Figure 3. Predicted overall monomer conversion profiles (grades A and B).

and a side one. The front feed stream was fed to the first reactor section, while the second stream was added to the inlet of the second reactor section. The initiator feed streams, consisting of mixtures of three peroxides, were introduced to the inlet of each reaction zone (see also Figure 1). The predictive capabilities of the mathematical model were examined by simulating several copolymer grades and comparing the model predictions with experimental measurements. In particular, the following copolymerizations were investigated: (i) ethylene–ethyl acrylate (EEA); (ii) ethylene–methyl acrylate (EMA); (iii) ethylene–vinyl acetate (EVA).

Ethylene–Acrylate (EA) Copolymers. Figures 2–7 illustrate some representative results for the EEA copolymerization. In particular, Figure 2 shows the scaled temperature profiles for two EEA copolymer grades. The continuous lines represent model predictions (obtained through the online parameter estimator modulus of the software), while the discrete points represent the experimental temperature measurements. It is apparent that the model predictions are in very good agreement with the measured temperatures. It should be pointed out that the two simulated copolymer grades correspond to significantly different operating conditions (e.g., initiator flow rates, coolant flow rates, etc.) and numbers of initiator injection points (e.g., two for grade A and three for grade B). Thus, the number of temperature peaks in the tube for grades A and B were two and three, respectively. Note that the monomer feed composition in ethyl acrylate was 4.6 wt % for

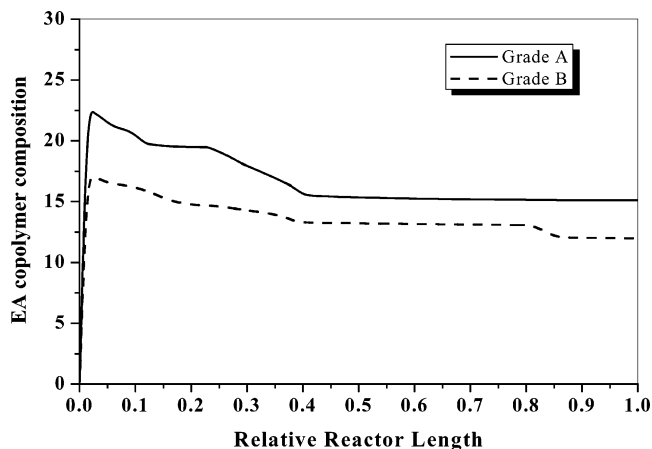


Figure 4. Predicted EA copolymer composition profiles (grades A and B).

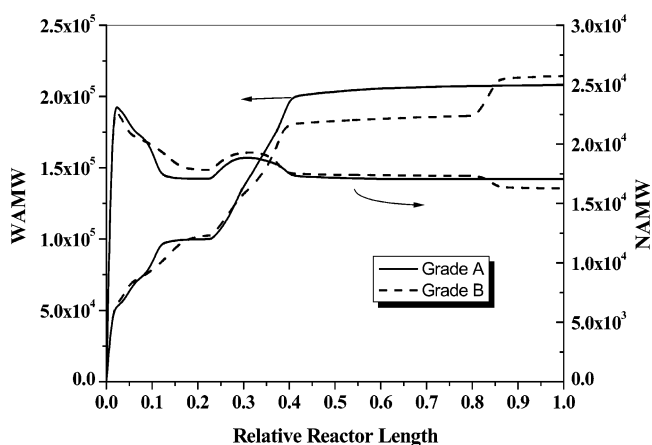


Figure 5. Predicted NAMW and WAMW profiles (grades A and B).

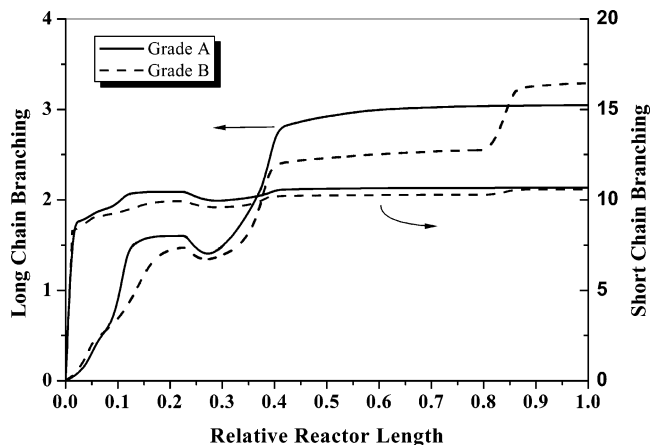


Figure 6. Predicted LCB and SCB profiles (grades A and B).

grade A and 3.5 wt % for grade B. In Table 2, predicted and measured results on number- and weight-average molecular weights, LCB, SCB, overall monomer conversion, and final copolymer composition are presented. The percentage error in the prediction of a property with respect to its experimental value is also reported. In general, model prediction errors are within the corresponding experimental measurement errors (e.g., ± 1 –15%).

In Figures 3–7, the overall monomer conversion, EA copolymer composition, number- and weight-average molecular weights, LCB, SCB, and amounts of vinyl and vinylidene are plotted with respect to the reactor length

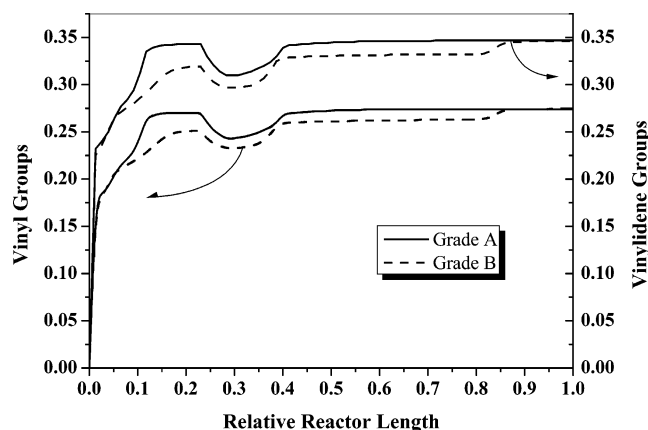


Figure 7. Predicted vinyl and vinylidene group profiles (grades A and B).

for grades A and B. In both cases, the predicted final conversion at the reactor exit is close to 27% (see Figure 3). On the other hand, the predicted final ethyl acrylate contents in the copolymer are 15.1 and 12.0 wt % for grades A and B, respectively, well above the respective monomer feed compositions. As discussed in the previous section in EA copolymerization, the acrylate content in the copolymer is significantly higher than the respective monomer feed composition because “live” polymer chains ending in an ethylene unit will favor cross-propagation reaction with the acrylate comonomer. As can be seen in Figure 4, the EA copolymer composition slowly decreases with the reactor length because of EA depletion.

In Figure 5, the number- and weight-average molecular weights are plotted with respect to the reactor length. Note that the number-average molecular weight (M_n) exhibits a small variation with the tube length. On the other hand, the weight-average molecular weight shows a large increase along the reactor length as a result of the increase of monomer conversion and, thus, of the rate of LCB formation. The LCB and SCB profiles along the tube are illustrated in Figure 6 for grades A and B. Note that the final number of LCB per 10^3 carbon atoms is about 3, while the final number of SCB per 10^3 carbon atoms is about 10.5. Finally, in Figure 7, the vinyl and vinylidene groups per 10^3 carbon atoms are plotted along the reactor length. The final predicted values for vinyl and vinylidene groups for both grades are 0.275 and 0.35, respectively. It should be noted that in the calculation of vinyl groups the contribution of transfer to monomer, solvent, and disproportionation reactions was not accounted for.

The capabilities of the online parameter estimator to capture the time-varying characteristics of the industrial reactor were also demonstrated by simulating the copolymerization of ethylene with methyl acrylate. The parameter estimation program described in the previous subsection was capable of reproducing the varying temperature profiles for EMA grades (D and E) through the estimation of the fouling factor and the initiator efficiency (Figure 8). It is apparent that model predictions (continuous lines) are in very good agreement with the measured temperature profiles (discrete points). For both grades, the monomer feed compositions in methyl acrylate in the front and side feed streams were 2.9 and 3.8 wt %, respectively. However, the operating peak temperatures for grade E were higher than those for grade D. As a result, the predicted overall monomer

conversion at the reactor exit for grade E was higher than that for grade D (i.e., 26.2 vs 23.6). Similarly, the predicted final values of M_n and M_w for grades E and D were (13 846, 393 730) and (15 283, 293 117), respectively. These results are in agreement with the predicted temperature profiles for grades E and D because higher polymerization temperatures result in a decrease of M_n and an increase of M_w due to the increase in the overall monomer conversion and LCB formation rate. Note that model predictions for the overall monomer conversion and copolymer composition are in excellent agreement with the corresponding experimental measurements (see Table 2).

It is important to mention that a postpeak reaction is observed in the second reaction-cooling section of the reactor. This means that copolymerization extends inside the cooling zones, which prolongs the copolymerization beyond the second temperature peak. This behavior was attributed to thermal initiation reactions and/or changes in the overall heat-transfer coefficient due to reactor fouling.

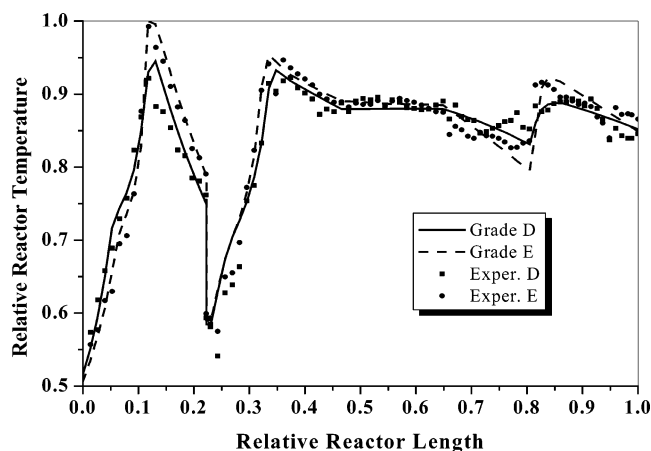
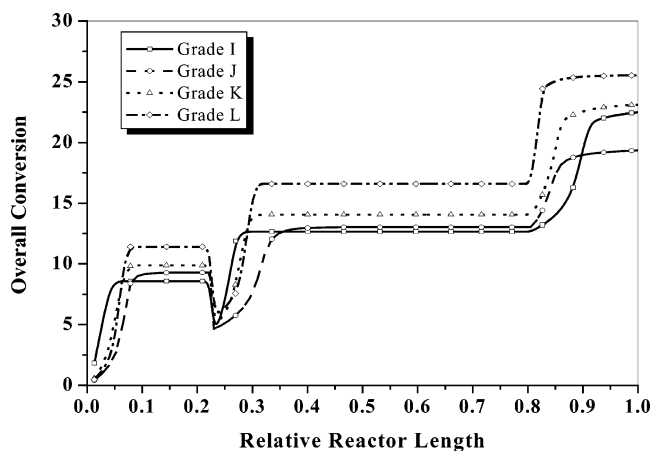
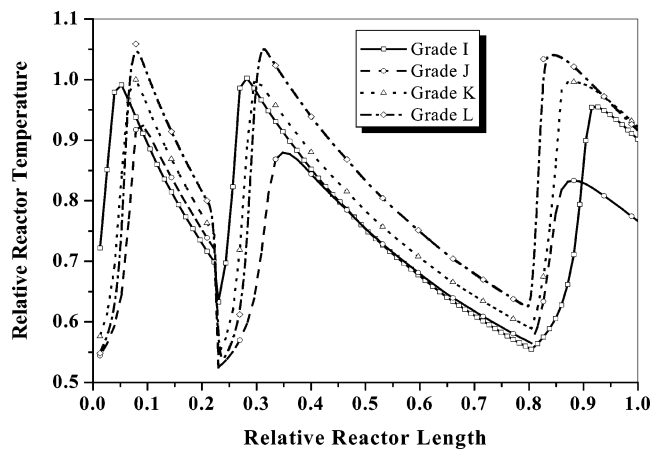
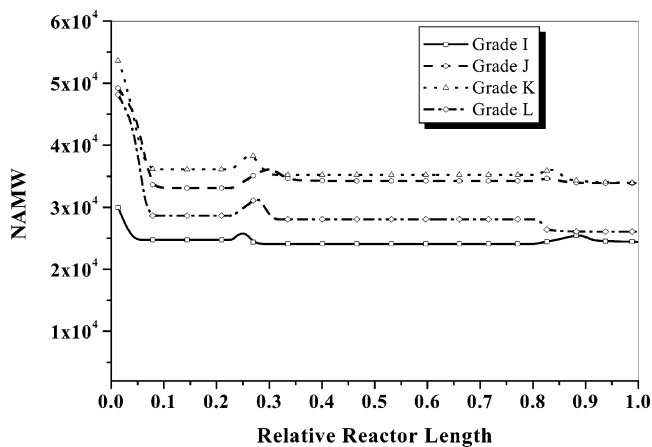
EVA Copolymers. Figures 9–14 illustrate some representative results for the EVA copolymerization. The VA contents in the feed composition streams were 28.15, 18.10, 12.1, and 18.10 wt % for the EVA grades I–L, respectively. For all of the investigated cases, the propylene and CTA mass fractions in the feed streams were equal [i.e., 0.28 (I), 0.30 (J), 0.31 (K), and 0.3 (L)]. The objective of this study was to find the operating conditions (i.e., maximum operating peak temperatures, concentrations, and flow rates of initiator mixtures, etc.) to achieve the product specifications and desired productivity (see Table 2) while satisfying the reactor operating constraints (e.g., available coolant maximum flow rates and min/max coolant temperatures, maximum polymerization temperature defined by the explosion decomposition temperature limits of EVA mixtures, reactor length, etc.). Thus, the experimental results for M_n , M_w , overall monomer conversion, and copolymer composition represent desired product specifications.

In Figure 9, scaled temperature profiles calculated for the production of EVA grades I–L are plotted with respect to the tube length. It is apparent that the peak positions and heights are very much related with the overall product specifications (e.g., desired M_n , M_w , conversion, and copolymer composition). By a comparison of the calculated temperature profiles for grades J and L (i.e., the same final copolymer composition but different values for M_n , M_w , and overall monomer conversion), it can be concluded that, in general, higher peak temperatures are required to increase the overall monomer conversion and weight-average molecular weight (see also Figures 10–12). On the other hand, by a comparison of the calculated temperature profiles for grades K and L (i.e., similar final conversions but different copolymer and molecular properties), it appears that the peak temperatures increase as the VA content in the copolymer increases.

In Figures 10–14, the overall monomer conversion, number- and weight-average molecular weights, LCB, and SCB per 10^3 carbon atoms are plotted with respect to the reactor length for grades (I–L). As can be seen, higher polymerization temperatures result in larger overall monomer conversions (Figure 10). Furthermore, as the VA content in the EVA increases, the number- and weight-average molecular weights are decreased (Figures 11 and 12). In all cases, the overall copolymer

Table 2. Copolymer Molecular Properties and Conversion (Predicted Results and Experimental Measurements)

grade	results	M_n	M_w	LCB	SCB	overall conversion	copolymer composition (%)
A (EEA)	pred	17 054	208 065	3.048	10.661	26.9	15.1
	exp	17 000	230 000			26.1	15.6
	% error	0.3	-9.5			3.1	-3.2
B (EEA)	pred	16 272	214 302	3.291	10.586	27.4	12.0
	exp	15 000	250 000			25.8	11.3
	% error	8.5	-14.3			6.2	6.2
D (EMA)	pred	15 283	293 117	4.861	9.946	23.6	9.7
	exp					23.8	9.5
	% error					-0.8	2.1
E (EMA)	pred	13 846	393 730	6.399	10.657	26.2	9.3
	exp					26.9	9.5
	% error					-2.6	-2.1
I (EVA)	pred	24 447	106 486	0.607	12.03	22.5	28.2
	exp	22 100	86 200			21.9	28
	% error	10.6	23.5			2.7	0.7
J (EVA)	pred	33 885	157 320	0.399	9.253	19.3	18.1
	exp	33 000	150 000			18.5	18
	% error	2.7	4.9			4.3	0.6
K (EVA)	pred	33 940	229 351	0.628	10.132	23.1	12.1
	exp	33 000	195 000			24.8	12
	% error	2.8	17.6			-6.8	0.8
L (EVA)	pred	26 065	203 651	0.792	11.407	25.5	18.1
	exp	25 550	176 748			25.1	18
	% error	2.0	15.2			1.6	0.6

**Figure 8.** Predicted vs measured temperature profiles for two EMA copolymer grades (D and E).**Figure 10.** Predicted overall monomer conversion profiles (grades I–L).**Figure 9.** Predicted temperature profiles for four EVA copolymers (grades I–L).**Figure 11.** Predicted NAMW profiles (grades I–L).

composition in VA remained constant along the tube length and approximately equal to the initial monomer feed composition because the reactivity ratios for ethylene and VA are approximately the same (see Table 1). Finally, in Figures 13 and 14, the SCB and LCB per 10^3 carbon atoms are plotted with respect to the reactor

length. In general, lower polymerization temperatures (i.e., low monomer conversions) result in a decrease of both structural properties. It should be pointed out that the errors in the model predictions of product specifications are within the acceptable range of analytical measurement errors (Table 2).

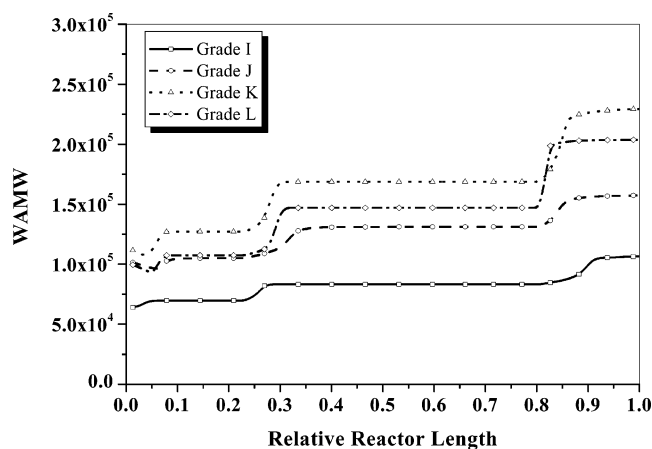


Figure 12. Predicted WAMW profiles (grades I–L).

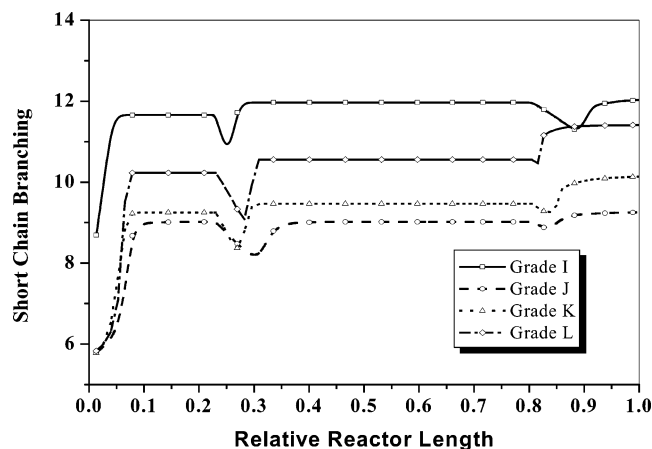


Figure 13. Predicted SCB profiles (grades I–L).

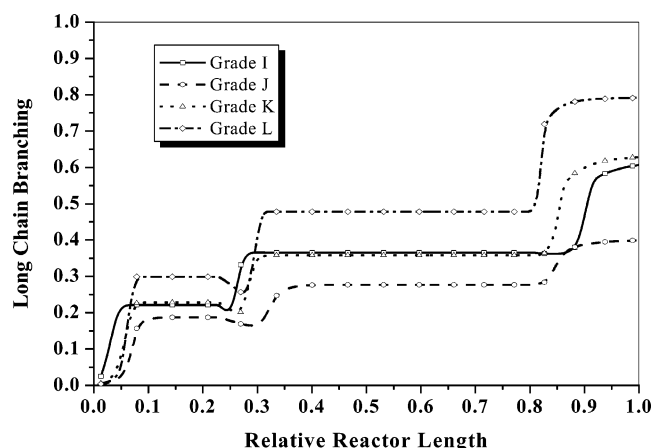


Figure 14. Predicted LCB profiles (grades I–L).

Conclusions

A user-friendly software package has been developed for the design, simulation, online parameter estimation, and optimization of industrial high-pressure, low-density ethylene copolymerization reactors. The design of the tubular reactor is flexible enough to allow the incorporation of alternative reactor configurations, multiple injection points for monomers, initiators, and solvents, and multiple coolant streams.

A detailed kinetic mechanism has been postulated to describe the free-radical copolymerization of ethylene with various comonomers. The method of double moments has been utilized to calculate the variation of all

of the molecular and structural copolymer properties (e.g., M_n , M_w , LCB, SCB, etc.) along the reactor length. The software tool includes a comprehensive library for the calculation of the thermodynamic and various transport properties of the reaction mixture in terms of the polymerization temperature, pressure, and composition of the mixture. A robust online parameter estimator has been developed, based on appropriate measurements from the reactor, to estimate key model parameters (i.e., the overall initiator efficiency and fouling factor in the reaction and cooling zones), which enables the online tuning of the model to real plant data. The key to this accomplishment is the comprehensiveness of the model and the knowledgeable selection of the tuning parameters.

The model capabilities were demonstrated by comparing model predictions with industrial measurements for a number of copolymer grades. Specifically, free-radical copolymerizations of ethylene with ethyl acrylate, methyl acrylate, and vinyl acetate monomers were studied. A wide range of operating conditions were employed to perform the model validation. Simulation results showed that model predictions were in very good agreement with experimental measurements on temperature profiles, overall monomer conversion, copolymer composition, and molecular weight averages for all of the examined cases. Note that the experimental verification of our simulation results on EVA grades is now in progress.

Acknowledgment

The authors gratefully acknowledge the financial support provided for this work by E. I. du Pont de Nemours and Company.

Notation

- A = reactor cross-sectional area, m^2
- A' = cross-sectional area of the reactor–jacket annulus, m^2
- C_j = molar concentration of the j th component, $kmol/m^3$
- C_p = reaction mixture heat capacity, $J/kg \cdot K$
- C_{pc} = coolant heat capacity, $J/kg \cdot K$
- $D_{p,q}$ = concentration of the “dead” copolymer chains with p monomer units of M_1 and q monomer units of M_2 , $kmol/m^3$
- d_i = inside tube diameter, m
- d_o = outside tube diameter, m
- E_v = activation energy for viscous flow, cal/mol
- F_j = molar flow rate of the j th component, $kgmol/s$
- f_i = efficiency of the i th initiator
- f_r = Fanning friction factor
- h_f = fouling coefficient, $kW/m^2 \cdot K$
- h_i = inside film heat-transfer coefficient, $kW/m^2 \cdot K$
- h_o = outside film heat-transfer coefficient, $kW/m^2 \cdot K$
- I_i = concentration of the i th initiator, $kgmol/m^3$
- k_{di} = decomposition rate constant of the i th initiator, s^{-1}
- k_{ti} = chain initiation rate constant for the i th monomer, $m^3/kgmol \cdot s$
- k_{thi} = thermal initiation rate constant for the i th monomer, $m^6/kgmol^2 \cdot s$
- k_{pij} = propagation rate constant of “live” polymer chains ending in the i th monomer unit with the j th monomer, $m^3/kgmol \cdot s$
- k_{tmij} = rate constant for the transfer of “live” polymer chains of type i to j monomer, $m^3/kgmol \cdot s$
- k_{tsij} = rate constant for transfer to the j th solvent of “live” polymer chains of type i , $m^3/kgmol \cdot s$
- k_{tpij} = rate constant for transfer to j “dead” polymer chains, $m^3/kgmol \cdot s$

k_{bi} = intramolecular chain transfer of "live" polymer chains of type i , s^{-1}

$k_{\beta i}$ = β -scission rate constant for secondary radicals, s^{-1}

$k_{\beta' i}$ = β -scission rate constant for tertiary radicals, s^{-1}

k_{teij} = termination by a combination rate constant, $m^3/kgmol \cdot s$

k_{tdij} = termination by disproportionation rate constant, $m^3/kgmol \cdot s$

LCB = number of long-chain branches per 10^3 carbon atoms

M_j = concentration of the j th monomer, $kgmol/m^3$

M_n = number-average molecular weight, $kg/kgmol$

M_w = weight-average molecular weight, $kg/kgmol$

M_z = z -average molecular weight, $kg/kgmol$

\dot{m}_c = coolant mass flow rate, kg/s

N_I = number of initiators

N_S = number of solvents

NAMW = number-average molecular weight, $kg/kgmol$

P = reactor pressure, atm

R^\bullet = concentration of primary radicals, $kgmol/m^3$

R_f = fouling of the reactor wall, $m^2 \cdot K/kW$

R^i = total concentration of "live" copolymer chains ending in a radical of type i

$R_{p,q}^i$ = concentration of "live" copolymer chains with p monomer units of M_1 and q

monomer units of M_2 ending in the i th terminal unit, $kgmol/m^3$

SCB = number of short-chain branches per 10^3 carbon atoms

S_k = concentration of the k th solvent, $kgmol/m^3$

T = reactor temperature, K

T_c = coolant temperature, K

U_i = overall heat-transfer coefficient, $kW/m^2 \cdot K$

V = reactor volume, m^3

VNL = number of vinyl double bonds per 10^3 carbon atoms

VND = number of vinylidene double bonds per 10^3 carbon atoms

WAMW = weight-average molecular weight, $kg/kgmol$

X_p = polymer weight fraction

Greek Letters

$-\Delta H_{ri}$ = heat of reaction for the i th monomer, $kJ/kgmol$

η_0 = reference solution viscosity at temperature T_0 , $kg/m \cdot s$

η_s = solution viscosity, $kg/m \cdot s$

η_{sp} = viscosity of monomers and solvents, $kg/m \cdot s$

$\lambda_{m,n}$ = double moments of "live" copolymer chains, $kgmol/m^3$

$\mu_{m,n}$ = double moments of "dead" polymer chains, $kgmol/m^3$

ρ_m = reaction mixture density, $kgmol/m^3$

Subscripts

b = backbiting

d = initiator decomposition

j = reactor jacket

p = propagation

tc = termination by combination

td = termination by disproportionation

tm = transfer to monomer

tp = transfer to polymer

ts = transfer to solvent

β = scission of secondary radicals

β' = scission of tertiary radicals

Literature Cited

- (1) Chou, R. T.; Keating, M. Y.; Hughes, L. J. High Flexibility EMA Made From High-Pressure Tubular Process. *Annu. Tech. Conf.—Soc. Plast. Eng.*, 60th **2002**, 2, 1832–1836.
- (2) Agrawal, S.; Han, C. D. Analysis of the High-Pressure Polyethylene Tubular Reactor with Axial Mixing. *AIChE J.* **1975**, 21 (3), 449–465.
- (3) Chen, C. H.; Vermeychuk, J. G.; Howell, J. A.; Ehrlich, P. Computer Model for Tubular High-Pressure Polyethylene Reactors. *AIChE J.* **1976**, 22 (3), 463.
- (4) Donati, G.; Marini, I.; Marziano, G.; Mazzaferrri, C.; Spampinato, M.; Langianni, B. Mathematical Model of Low-Density Polyethylene Tubular Reactor. *ACS Symp. Ser.* **1982**, 196, 579.
- (5) Goto, S.; Yamamoto, K.; Furui, S.; Sugimoto, M. Computer Model for Commercial High-Pressure Polyethylene Reactor Based on Elementary Reaction Rates Obtained Experimentally. *J. Appl. Polym. Sci., Appl. Polym. Symp.* **1981**, 36, 21–40.
- (6) Yoon, B. J.; Rhee, H.-K. A Study of the High-Pressure Polyethylene Tubular Reactor. *Chem. Eng. Commun.* **1985**, 34, 253–265.
- (7) Kiparissides, C.; Mavridis, H. Optimization of a High-Pressure Polyethylene Tubular Reactor. *Polym. Process Eng.* **1985**, 3 (3), 263–290.
- (8) Gupta, S. K.; Kumar, A.; Krishnamurthy, M. V. G. Simulation of Tubular Low-Density Polyethylene. *Polym. Eng. Sci.* **1985**, 25, 37.
- (9) Feucht, P.; Tilger, B.; Luft, G. Prediction of Molar Mass Distribution, Number and Weight Average Degree of Polymerization and Branching of Low-Density Polyethylene. *Chem. Eng.* **1985**, 40 (10), 1935–1942.
- (10) Shirodkar, P.; Tsien, G. O. A Mathematical Model for the Production of Low-Density Polyethylene in a Tubular Reactor. *Chem. Eng. Sci.* **1986**, 41 (4), 1031–1038.
- (11) Brandolin, A.; Capiati, N. J.; Farber, J. N.; Valles, E. M. Mathematical Model for High-Pressure Tubular Reactor for Ethylene Polymerization. *Ind. Eng. Chem. Res.* **1988**, 27, 784–790.
- (12) Brandolin, A.; Lacunza, M. H.; Ugrin, P. E.; Capiati, N. J. High-Pressure Polymerization of Ethylene. An Improved Mathematical Model for Industrial Tubular Reactors. *Polym. React. Eng.* **1996**, 4 (4), 193–241.
- (13) Zabinsky, R. C. M.; Chan, W. M.; Gloor, P. E.; Hamielec, A. E. A Kinetic Model for Olefin Polymerization in High-Pressure Tubular Reactors: A Review and Update. *Polymer* **1992**, 33 (11), 2243–2262.
- (14) Verros, G.; Papadakis, M.; Kiparissides, C. Mathematical Modeling of High-Pressure Tubular LDPE Copolymerization Reactors. *Polym. React. Eng.* **1993**, 1 (3), 427–460.
- (15) Kiparissides, C.; Verros, G.; MacGregor, J. F. Mathematical Modeling, Optimization, and Quality Control of High-Pressure Ethylene Polymerization Reactors. *J. Macromol. Sci., Rev. Macromol. Chem. Phys.* **1993**, C33 (4), 437–527.
- (16) Becker, P.; Busch, M. Modeling of Ethylene Copolymerizations with Acrylate Comonomers. *Macromol. Theory Simul.* **1998**, 7, 435–446.
- (17) Van Bortel, M. H. C. M.; Busch, A. General Model Describing Molecular Weight Distributions and Branching Indices in Copolymerizations Demonstrated by the High-Pressure Free-Radical Copolymerization of Ethene and Methyl Acrylate. *Macromol. Theory Simul.* **2001**, 10, 25–37.
- (18) Busch, A. Modeling Kinetics and Structural Properties in High-Pressure Fluid Phase Polymerization. *Macromol. Theory Simul.* **2001**, 10, 408–429.
- (19) Pladis, P.; Kiparissides, C. A Comprehensive Model for the Calculation of Molecular Weight and Long Chain Branching Distribution in Free-Radical Polymerizations. *Chem. Eng. Sci.* **1998**, 53 (18), 3315–3333.
- (20) Arriola, D. J. Modeling of Addition Polymerization Systems. Ph.D. Thesis, University of Wisconsin, Madison, WI, 1989.
- (21) Lee, B. I.; Kesler, M. G. A Generalized Thermodynamic Correlation Based on Three-Parameter Corresponding States. *AIChE J.* **1975**, 21 (3), 510–527.
- (22) Maloney, D. P.; Prausnitz, J. M. Thermodynamic Properties of Liquid Polyethylene. *J. Appl. Polym. Sci.* **1974**, 18, 2703.
- (23) Mendelson, R. A. A Method for Viscosity Measurement of Concentrated Polymer Solutions in Volatile Solvents at Elevated Temperatures. *J. Rheol.* **1979**, 23 (5), 545.

- (24) Mendelson, R. A. Concentrated Solutions Viscosity Behavior in Volatile Solvents at Elevated Temperatures Polystyrene in Ethylbenzene. *J. Rheol.* **1980**, *24* (6), 765.
- (25) Reid, R.; Prausnitz, J.; Poling, B. *The Properties of Gases and Liquids*, 4th ed.; McGraw-Hill: New York, 1988; p 424.
- (26) Ehrlich, P.; Woodbrey, J. Viscosities of Moderately Concentrated Solutions of Polyethylene in Ethane, Propane, and Ethylene. *J. Appl. Polym. Sci.* **1969**, *13*, 117–131.
- (27) Brodkey, R. S.; Hershey, H. C. *Transport Phenomena. A Unified Approach*; McGraw-Hill: New York, 1988.
- (28) Buback, M.; Droge, T.; van Herk, A.; Mahling, F. High-Pressure Free-Radical Copolymerization of Ethene and 2-Ethylhexyl Acrylate. *Macromol. Chem. Phys.* **1996**, *197*, 4119–4134.
- (29) Buback, M.; Droge, T. High-Pressure Free-Radical Copolymerization of Ethene and Methyl Acrylate. *Macromol. Chem. Phys.* **1997**, *198*, 3627–3638.
- (30) Buback, M.; Wittkowski, L.; Lehmann, S. A.; Mahling, F. O. High-Pressure Free-Radical Copolymerization of Ethene–Methacrylic Acid and of Ethene–Acrylic Acid. 1. (Meth)acrylic Acid Reactivity Ratios. *Macromol. Chem. Phys.* **1999**, *200*, 1935–1941.
- (31) Buback, M.; Wittkowski, L. High-Pressure Free-Radical Copolymerization of Ethene with Methacrylic Acid and Ethene with Acrylic Acid. 2. Ethene Reactivity Ratios. *Macromol. Chem. Phys.* **2000**, *201*, 419–426.
- (32) Buback, M.; Busch, M.; Lovis, K.; Mahling, F. High-Pressure Free-Radical Copolymerization of Ethene and Butyl Acrylate. *Macromol. Chem. Phys.* **1996**, *197*, 303–313.
- (33) Buback, M. The High-Pressure Polymerization of Pure Ethylene. *Macromol. Chem.* **1980**, *181*, 373–382.
- (34) Buback, M. Free-Radical Polymerization up to High Conversion. A General Kinetic Treatment. *Macromol. Chem.* **1990**, *191*, 1575–1587.
- (35) Keramopoulos, A.; Kiparissides, C. Development of a Comprehensive Model for Diffusion Controlled Free-Radical Copolymerization Reactions. *Macromolecules* **2002**, *35*, 4155–4166.
- (36) Kiparissides, C.; Verros, G.; Pertsinidis, A.; Goosens, I. On-line Parameter Estimator in a High-Pressure Low-Density Polyethylene Tubular Reactor. Computer Aided Design of Polymer Reactors. *AIChE J.* **1996**, *42* (2), 440–454.
- (37) *IMSL Math Library, Visual Numerics*; Houston, Texas, 1997; p 878.

Received for review May 13, 2004

Revised manuscript received August 26, 2004

Accepted August 30, 2004

IE049596F